Ultrasonics Sonochemistry 19 (2012) 560–569

Contents lists available at SciVerse ScienceDirect

Ultrasonics Sonochemistry

journal homepage: www.elsevier.com/locate/ultsonch

A novel approach for the synthesis of superparamagnetic Mn_3O_4 nanocrystals by ultrasonic bath

T. Rohani Bastami, M.H. Entezari *

Department of Chemistry, Ferdowsi University of Mashhad, 91775, Mashhad, Iran

ARTICLE INFO

Article history:
Received 9 August 2011
Received in revised form 3 October 2011
Accepted 18 October 2011
Available online 24 October 2011

Keywords:
Husmannite
Nanorod
Superparamagnetic
Ferrimagnetic
Ultrasonic irradiation
Basic media

ABSTRACT

In this study, the synthesis of Mn_3O_4 (husmannite) nanoparticles was carried out in two different alkali media under sonication by ultrasonic bath and conventional method. Manganese acetate was used as precursor, sodium hydroxide and hexamethylenetetramine (HMT) as basic reagents in this synthesis. An ultrasonic bath with low intensity was used for the preparation of nanomaterials. The as prepared samples were characterized with X-ray diffraction (XRD), Fourier transform infrared (FTIR) spectroscopy, transmission electron microscopy (HRTEM, TEM), energy-dispersive spectrum (EDS), and superconducting quantum interference device (SQUID) analysis. The XRD patterns exhibit the nanocrystals are in pure tetragonal phase. The chemical composition was obtained by EDS analysis and confirmed the presence of Mn and O in the sample. According to the TEM and HRTEM results, both nanorods and nanoparticles of Mn_3O_4 were obtained in the presence of ultrasonic irradiation. The average size of nanoparticles was 10 nm, and the size of nanorods was 12 nm in diameter and 100–900 nm in length for the samples prepared in basic medium with sodium hydroxide. In the conventional method with the same basic medium, the nanorod was not observed and the nearly cubic nanoparticles was appeared with an average size of 2.5 nm. The selected area electron diffraction (SAED) patterns revealed that the nanocrystals are polycrystalline in nature. When HMT was used as a basic reagent in the presence of ultrasonic irradiation, it was led to a higher size of nanoparticles and nanorods than when sodium hydroxide was used as a basic reagent. The average size of nanoparticles was about 15 nm and its shape was nearly cubic. The diameter for nanorods was 50 nm and the length was about a few micrometers.

The magnetic measurements were carried out on the sample prepared in sodium hydroxide under ultrasonic irradiation. These measurements as a function of temperature and field strength showed a reduction in ferrimagnetic temperature (T_c = 40 K) as compared to those reported for the bulk (T_c = 43 K). The superparamagnetic behavior was observed at room temperature with no saturation magnetization and hysteresis in the region of measured field strength.

1. Introduction

A great deal of attention has been paid to the synthesis of soft magnetic materials which have been extensive applications in electronic and information technologies [1]. Magnetism of materials in the nanosize scale is of extreme importance due to their potential applications in different fields such as high-density recording media, ferrofluid technology, magnetic resonance imaging, etc. [2–5]. When the crystallite sizes of magnetic material reduce to a few nanometers, energy considerations favor the formation of single domain particles, which could exhibit unique properties such as superparamagnetism [6,7].

Up to now, researchers have proposed several synthesis approaches such as co-precipitation [8], sol–gel [9], hydrothermal method [10], thermal decomposition [11], solvothermal method [12], and microwave assisted method [13]. However, most of these approaches contain multi-step synthetic processes or protection from oxygen, involving unfavorably high growth temperatures and long reaction times. Currently, there is a trend toward simple, low temperature solution method for the nanoparticle preparation. One of the novel and simple method for the synthesis of nanomaterial in the low temperature is sonochemistry [14–17]. Sonochemistry as an effective and powerful technique is used for the synthesis of different compound in the normal condition. Sonochemically synthesized materials are highly active in catalysis due to their particles size and high surface area [18]. The chemical effects of ultrasound appear from acoustic cavitations, that is, the formation, growth and implosive collapse of bubbles in a liquid [19]. The implosive collapse of the bubbles generates a localized hot spot through adiabatic compression or shock wave formation within the gas phase of the collapsing bubble. The conditions

* Corresponding author.
E-mail address: moh_entezari@yahoo.com (M.H. Entezari).

1350-4177/$ - see front matter © 2011 Elsevier B.V. All rights reserved.
doi:10.1016/j.ultsonch.2011.10.012

formed in these hot spots have been experimentally determined, with transient temperatures of ~5000 K, pressure of 1800 atm and cooling rates in excess of 10^{10} K/s [19]. Most of the research for the synthesis of nanomaterials was focused on the preparation of nanomaterials by using high intensity ultrasonic probe [20–22].

There are different fabrications of magnetic nanocrystals with different morphology. Most of them focused on the synthesis of 3D spherical nanoparticles. In the past few years great efforts have been developed to the fabrication of 1D nanomaterials like vapor deposition [23], solvothermal reaction [24], and surfactant-assisted method [25] for their unique properties. Ultrasonic irradiation could offer an attractive method for the preparation of 1D nanomaterial [26–29]. Owing to more efficient mixing [30] and faster mass transfer of the reactants [31] under action of microjet and shock wave of the ultrasound, the proper use of ultrasonic irradiation can significantly improve crystal nucleation and growth. The ultrasonic wave probably has the ability to improve oriented-attachment of primary nanoparticles and lead to 1D nanoparticle [27].

Spinel oxides having the general form of AB_2O_4, offer a rich system for the study of complex magnetic order. Both the tetrahedral A sites ion and the octahedral B sites ion can be magnetic [32,33]. One of the magnetic spinel materials is Mn_3O_4 with spinel structure. Mn_3O_4 is a complex oxide of manganese containing both di- and tri-valent manganese. The formula can be represented as $Mn^{2+}(Mn^{3+})_2O_4$, which Mn^{3+} is in octahedral position and Mn^{2+} is in tetrahedral position of the spinel structure [34]. Bulk Mn_3O_4 exhibits a tetragonal Jahn–Teller distortion at the Mn^{3+} site at high temperature to the $I4_1/amd$ space group [35]. The synthesis of Mn_3O_4 has gained significant attention due to its wide range applications, such as high density magnetic storage media, catalysts, ion exchange, molecular adsorption, electrochemical materials, solar energy transformation, and soft magnetic materials [36–41]. Mn_3O_4 has also been shown different applications in industry such as catalyst for oxidation of CH_4, the selective reduction of nitrobenzene, the decomposition of waste NO_x [42–46], the oxidation of C3 organic compound like propane, propene, acetone, acrolein [47], as a pigment [48], and in batteries [49]. The nanometer sized Mn_3O_4 powder with remarkably increased surface area and different morphologies are expected to display better performance in the all-above mentioned applications. There are many works which reported the synthesis of Mn_3O_4 with classical and solvothermal methods [50,51]. These methods require long reaction time in the range of 12–72 h at different temperatures and pressures. Another method which was used for the preparation of Mn_3O_4 is sol–gel [52]. This method has been known to be expensive, time consuming, and polluting. The conventional high-temperature calcinations for preparation of Mn_3O_4 lead to inconsistency in product quality and it is uneconomical [53]. Ozkaya et al. [53] were used an oxidation–precipitation method based on the oxidation of manganese sulfate and hydrolyzing with NaOH and concentrated NH_3 at 100 °C using stirrer method [53]. Sodium nitrate solution was added into the reaction mixture dropwise for overnight. They found that the samples obtained by NaOH were spherical with average size of (14 ± 5) nm and the samples obtained by using NH_3 were a mixture of spherical and ellipsoids [53]. Li et al. [54] have synthesized Mn_3O_4 with average size of 10 nm via esterification process with alcohol and $Mn(Ac)_2$,4 H_2O in the range of 90–150 °C. Chen et al. [55] have synthesized different morphologies of Mn_3O_4 (nanoparticles, nanorods, and nanofractals) by control the dropping speed of NaOH solution. Yang et al. [56] were obtained (1-D) nanorods of Mn_3O_4 using high temperature calcination of γ-MnOOH. Mn_3O_4 nanowires were obtained via solvothermal treatment of γ-MnOOH in polypropylene glycol at 180 °C for 24 h [57]. Park and co-workers synthesized Mn_3O_4 nanoparticles by decomposition of $[Mn(acac)_2]$ (acac = acetylacetonate) in oleylamine at 180 °C [58]. Qian and co-workers [59] have synthesized Mn_3O_4 nanorods in alcohol–water mixtures, using $KMnO_3$ as a starting manganese source and Na_2SO_3 as a reducing agent at 140 °C. Also, Mn_3O_4 nanorods with an average width and length of 6.6 ± 1.2 nm and 17.4 ± 4.1 nm were obtained by using $Mn(Ac)_2$, $4H_2O$ in DMF-H_2O media for aging time of 3 months [60]. In the other research work, different manganese salts were used for the synthesis of Mn_3O_4 nanoparticles via solvothermal reaction in DMF as solvent. The size of Mn_3O_4 nanocrystals was 22.5 ± 7.3 nm and 7.3 ± 1.4 nm prepared using $MnCl_2$ and $Mn(CH_3COO)_2$, respectively, at 160 °C for 24 h [61]. Also, Mn_3O_4 nanoparticles were obtained using polyol process by using $Mn(CH_3COO)_2$ as precursors and diethylene glycol [62].

There are some works about the synthesis of Mn_3O_4 with ultrasonic irradiation using high intensity ultrasonic probes [63–65]. But there is no report regarding to the synthesis of Mn_3O_4 nanoparticles by using ultrasonic bath as a low power ultrasonic irradiation. Gopalakrishnan et al. [63] synthesized Mn_3O_4 nanoparticles with an average size of 15 nm using high intensity ultrasonic irradiation. They used Mn acetate as precursor in neutral media. Rohani and Entezari [64] reported the synthesis of Mn_3O_4 nanoparticles with average size of 4 nm via high intensity ultrasonic irradiation in neutral media with Mn acetate as precursor. Gedanken and co-workers prepared 30–40 nm Mn_3O_4 nanoparticles with Mn acetate as precursor in basic media (pH 8.3) by using high intensity ultrasonic irradiation [65]. There is no report about the formation of Mn_3O_4 nanorods using high intensity ultrasonic irradiation.

This study focuses on the synthesis of Mn_3O_4 nanoparticles by using ultrasonic cleaning bath as a low power source of irradiation. Based on our knowledge, there is no report up to now about the synthesis of Mn_3O_4 in such a low power ultrasonic irradiation and mild conditions. Nanocrystalline Mn_3O_4 was obtained by two different basic reagents at pH 8.0 and compared with the conventional method. It was shown that ultrasonic irradiation can be led to nanorod structure in normal conditions without any further post treatment.

2. Experimental

2.1. Material

Manganese(II) acetate $4H_2O$, sodium hydroxide, and hexamethylenetetramine were purchased from Merck Company. Mili-Q water was used with a resistivity not less than 18.2 MΩ cm^{-1}.

2.2. Procedure

In all experiments, 4.6 g of manganese acetate was dissolved in about 30 mL of mili-Q water and the temperature was adjusted at 60 ± 2 °C with aging time of 180 min. In the temperature below 60 °C, the induction period for the formation of the particles was very long. The pH of solution was controlled at 8.0 by adding of sodium hydroxide or adding 7.2 g of HMT in the manganese acetate solution. The sodium hydroxide solution was added dropwise to control the pH (1 drop/min) of solution before sonication. The prepared solution was transferred into an erlenemayer as a reaction vessel and placed on the top of the water in ultrasonic bath. All experiments were carried out in ambient conditions under air atmosphere. It is important to find the optimum position of the reaction vessel in the bath. The simplest method is to locate the vessel horizontally on the top of the water where it shows the maximum disturbance on the surface of liquid inside the vessel. The same erlenemayer was used each time since differences in the thickness of vessel can affect on the ultrasonic power transfer into the reaction ves-

sel. The amount of acoustic power reaches to the reaction is normally low between 1 and 5 W/cm^2 [66]. In the conventional method, the prepared solution was stirred vigorously instead of ultrasonic irradiation and the other conditions were the same as sonication method.

Two experiments were run by rapidly and dropwise (1 drop/min) addition of NaOH solution (10%, w/v) into manganese acetate solution to pH 8.0. The obtained precipitates before and after sonication with ultrasonic bath were characterized by FTIR.

2.3. Characterization and instrument

The size and morphology of the Mn_3O_4 were characterized using a JEOL-2010 TEM operating at 200 kV of accelerate voltage. The TEM (LEO 912 ab, ziess Germany, 120 kV) was also used for the characterization of the product. The sample was dispersed in ethanol and dropped on the copper grid before loading to the instrument. The XRD of Mn_3O_4 was recorded on Bruker, D8ADVANCE, Germany (X-ray Tube Anode: Cu, Wavelength: 1.5406 Å (Cu Kα) Filter: Ni). The FTIR of the samples were recorded using Nicolet 6700 in the range of 400–4000 cm^{-1} with ATR accessories. The magnetization measurements were carried out using a Magnetic Property Measure System (MPMS, Quantum design) under magnetic fields up to 10000 Oe at 300 K and 10 K.

The ammonia concentration from decomposition of urotropin (HMT) was measured by UV–visible spectrophotometer (Unico 2800) through the addition of nessler reagent to the solution.

The ultrasonic equipment used for the synthesis of nanomaterials was a Branson 8510E-DTE ultasonic bath which is commonly used for the cleaning purposes in different laboratories (40 kHz-overall dimensions: 24 in. × 18 in. × 14.5 in.; internal dimensions: 19.5 in. × 11.5 in. × 6 in.).

2.4. Calorimetry

The real transducer's efficiency for electrical to sound conversion which is called acoustic power was determined by calorimetric method. Since the ultrasonic irradiation of a liquid produces heat, recording the temperature as a function of time leads to the acoustic power estimation by the following equation [67]:

$$P = m \cdot C_p \cdot \left(\frac{dT}{dt}\right) \quad (1)$$

where, m is the mass of the sonicated liquid (g), C_p is the specific heat of medium (water, 4.2 J (g K)$^{-1}$), and dT/dt is the temperature rise per second.The ultrasonic intensity of bath sonicator at 30 °C was 0.30 W cm^{-2} and the ultrasonic density was 0.011 W cm^{-3}.

2.5. Formation of H_2O_2

Hydrogen peroxide concentration was determined iodometrically [68]. In this method, iodide ion is oxidized by H_2O_2 in neutral or slightly acidic solutions. The iodide reagent was prepared immediately before use by mixing equal volumes (1.25 mL) of solution A (6.6 g of KI, 0.2 g of NaOH, 0.02 g of $(NH_4)_6Mo_7O_{24} \cdot 4H_2O$ in 100 mL of mili-Q water) and solution B (2 g of potassium hydrogen phthalate in 100 mL of mili-Q water). The sample solution (2 mL) was added to the described mixture of solution. Then, the absorption of I_3^- was measured at 351 nm. By measuring the concentrations at different times, the rate of formation of H_2O_2 was 0.752 μM min^{-1} at 60 °C.

2.6. Sono-decomposition of HMT

HMT was used as a generator of hydroxyl ions. It is well-known that HMT produces OH^- ions in solution according to the following reactions:

$$(CH_2)_6N_4 + 6H_2O \rightarrow 4NH_3 + 6HCHO \quad (2)$$

$$NH_3 + H_2O \rightarrow NH_4^+ + OH^- \quad (3)$$

The decomposition of HMT in the presence of ultrasonic irradiation was followed by dissolving 7.2 g of HMT in 30 mL of mili-Q water. The prepared solution was transferred into an erlenemayer as a reaction vessel and placed on the top of the water in ultrasonic bath as described above. The aging temperature and aging time were 60 ± 2 °C and 1 h. The concentration of ammonia in a sample was determined by addition of nessler reagent according to the following equation [69,70]:

$$2(HgI_2 \cdot 2KI) + NH_4OH + 3NaOH \rightarrow OHg_2NH_2I + 3H_2O + 4KI + 3NaI \quad (4)$$

The addition of nessler reagent led to a color from yellow to brown based on the concentration of ammonia. The measurement was carried out at the wavelength of 480 nm.

3. Results and discussion

3.1. X-ray analysis

The crystalline nature of the samples obtained in the presence and absence of ultrasonic irradiation was confirmed by XRD analysis (Supplementary Figs. S1 and S2). These samples were prepared in basic medium (pH 8.0) by NaOH, and HMT separately. It reveals that the XRD peaks in the patterns can be indexed to the (101), (112), (103), (211), (220), and (224) for tetragonal husmannite (Mn_3O_4) structure in accordance with JCPDS card of Mn_3O_4 (JCPDS-24-0737). There were no impurity phases in the samples prepared in the presence and absence of ultrasonic irradiation. The strong intensity and narrow width of diffraction peaks indicate that the resulting products are in a high crystallinity especially in the case of sample obtained by HMT. In addition, the narrower diffraction peaks of the sample in the case of HMT indicate the particle size should be rather larger. The lattice parameters of the nanoparticles under two different media were determined (Table S1). In all cases, the samples synthesized in the presence of ultrasonic irradiation had smaller lattice parameters than conventional method.

3.2. FTIR analysis

The FTIR analysis was performed and the spectra were presented in Fig. 1. Two significant absorption peaks are observed in the range of 450–650 cm^{-1}. The vibration frequency at 602 cm^{-1} is the characteristic of Mn–O stretching mode in tetrahedral sites, whereas vibration band located at a lower wavenumber, 480 cm^{-1}, can be attributed to the distortion vibration of Mn–O in an octahedral environment [53,71]. The peak in the range of 3300–3500 cm^{-1} is related to the adsorbed water on the samples and hydroxyl groups on the surface of nanoparticle.

The FTIR analysis of the precipitates obtained by rapidly and dropwise addition of NaOH solution before sonication was performed (Supplementary Fig. S3). In the case of rapidly added NaOH, the broad peak at 2600–3600 cm^{-1} is due to adsorbed water molecules and O–H stretching band. The two peaks at 1440 cm^{-1} and 1580 cm^{-1} can be assigned to υ_{C-O} (sym) and υ_{C-O} (asym). It is suggested that these two peaks are related to the adsorption of

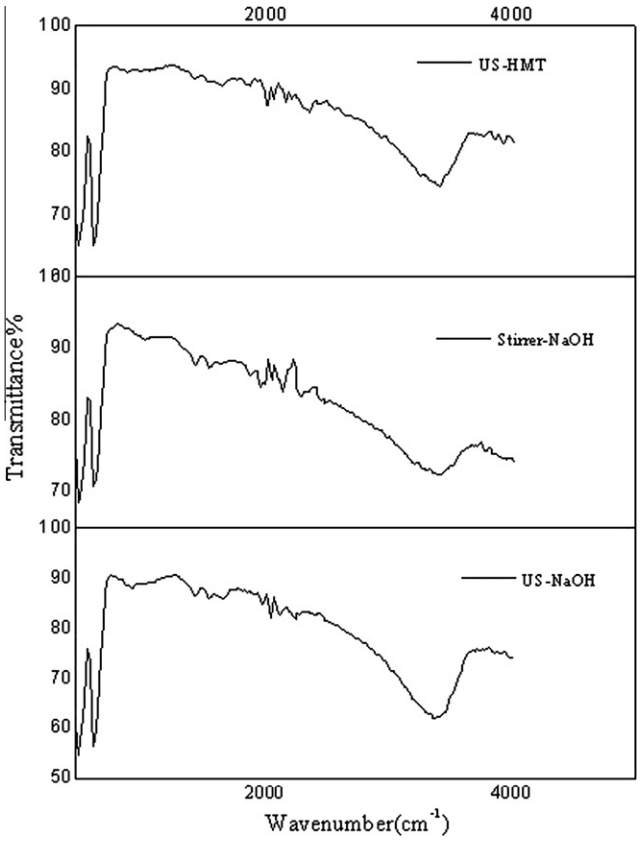

Fig. 1. FTIR spectrum of the Mn_3O_4.

acetate anion on the surface of precipitates. The peak at 644 cm^{-1} may be related to the vibration band of Mn–O. In the case of dropwise added NaOH, the peaks at 1417 cm^{-1}, 1568 cm^{-1}, and 1627 cm^{-1} are owing to the symmetric and asymmetric vibration of C–O from adsorbed acetate anions on the surface of precipitate too. In this case, two peaks at 630 cm^{-1} and 527 $cm^{-1}$are related to the Mn–O vibration bands.

The FTIR analysis was also carried out on the precipitates formed with rapidly and dropwise added of NaOH and then sonicated by ultrasonic bath (Supplementary Fig. S4). In the case of sample obtained by rapidly added of NaOH, there is one peak around 658 cm^{-1} which is related to Mn–O vibration mode. But, in the case of dropwise addition of NaOH, two peaks are observed at 602 cm^{-1} and 480 cm^{-1}. These observations confirm that the rate of alkaline addition can affect on the chemical structure of the products.

3.3. Morphology, size, and size distribution

Fig. 2 (a) and (b) shows the TEM images of Mn_3O_4 nanocrystals synthesized by NaOH using ultrasonic bath. These images confirm the sample consist of nearly cubic nanoparticles with average size of 10 nm and some rod-like structure. The diameter of rod-like was around 12 nm and its length was in the range of 100–900 nm. Some of the particles were attached to the surface of nanorods.

The HRTEM image, the corresponding SAED pattern, and the lattice image of the sample under the ultrasound are shown in Fig. 3(a)–(d). The observed lattice spacing of 2.6 Å and 2.9 Å correspond to the (103) and (112) planes of tetragonal Mn_3O_4, respectively. The SAED pattern reveals the nanocrystals are polycrystalline in nature. The size of nanoparticle according to the HRTEM image was found to be about 10 nm. The size distribution was obtained from the HRTEM image and confirms the nearly uniform size of the samples.

The chemical composition of the nanoparticles has been analyzed using EDS analysis as shown in Fig. 4. The Cu peaks are the signal detected from the TEM grid. This result confirms the presence of Mn and O in the nanopowder.

In the case of conventional method, the HRTEM images and the lattice spacing of Mn_3O_4 nanoparticles are presented in Fig. 5(a)–(c). According to these results, no nanorods were obtained in the absence of ultrasonic irradiation, and the average size of nearly cubic nanoparticles was 2.5 nm. Based on the SAED pattern which is shown in Fig. 5d, the structure of nanoparticles is polycrystalline in nature. The observed lattice spacing of 2.0 Å, 2.4 Å, and 1.5 Å correspond to the (220), (211), and (224) planes of tetragonal Mn_3O_4, respectively. The size distribution of the samples confirms the nearly uniform size of nanocrystals. The EDS analysis confirms the presence of O and Mn elements in the sample (Fig. 6).

The increase of particle size and the formation of nanorods in the presence of ultrasonic waves can be explained by the two following statements:

(1) It has suggested that NaOH has a strong adsorption on the surface of nanoparticles [72,73]. This strong capping agent on the surface of nanoparticles hinders the Ostwald ripening growth. Therefore, the size of nanoparticles cannot increase significantly. It is assumed that ultrasonic waves can be led to an irreversibly desorption of capping agents (NaOH) from the surface of nanoparticles by cavitational collapse. For this reason, a larger size of nanoparticles can be observed in the presence of ultrasonic irradiation.
(2) For the diffusion-controlled crystal growth, it has suggested that each crystal is surrounded by a diffusion sphere [74]. It is proposed that ultrasonic irradiation promotes the mass

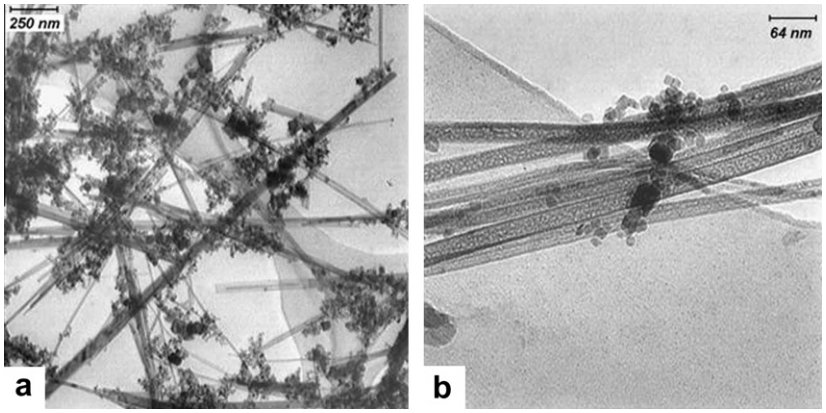

Fig. 2. (a, b) TEM images of Mn_3O_4 nanocrystal using ultrasonic irradiation (NaOH).

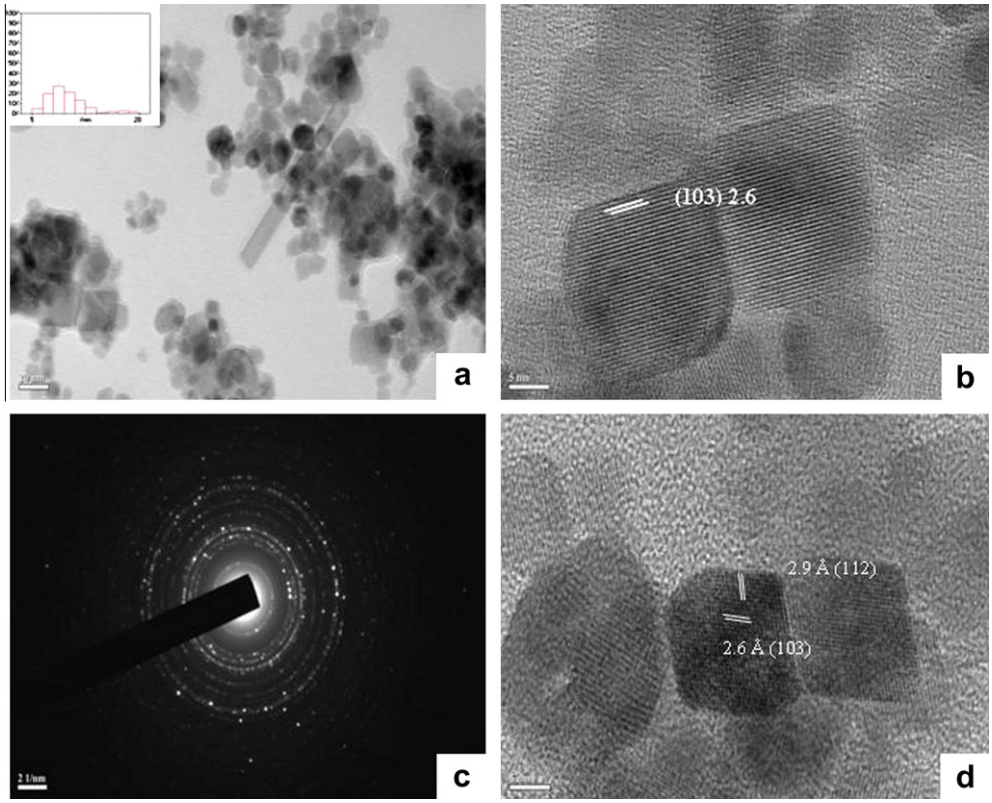

Fig. 3. (a) HRTEM, (b, d) lattice image, and (c) SAED pattern of Mn_3O_4 nanocrystal using ultrasonic irradiation (NaOH).

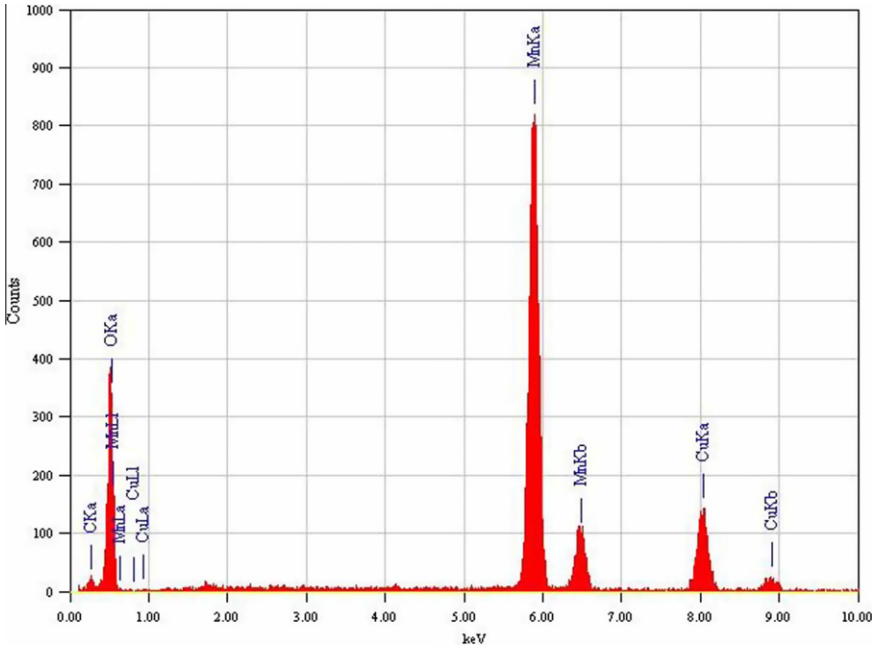

Fig. 4. EDS pattern of Mn_3O_4 nanocrystal using ultrasonic irradiation (NaOH).

transfer and diffusion of precursors from the bulk into the diffusion sphere, so the facets along the axis which are more active should be quickly grow and led to the production of 1D structure. Another important parameter is the thickness of the diffusion sphere which is reduced by ultrasonic irradiation and this leads to an increase of flux diffusion and faster growth along the active axis.

In addition, under sonication, an oriented attachment process can be occurred by mechanism of alignment and coalescence between the particles. Since it has suggested the oriented attachments may occur via collisions of aligned nanoparticles in suspension or rotation of misaligned nanoparticles in contact toward low-energy interface configuration [75,76].

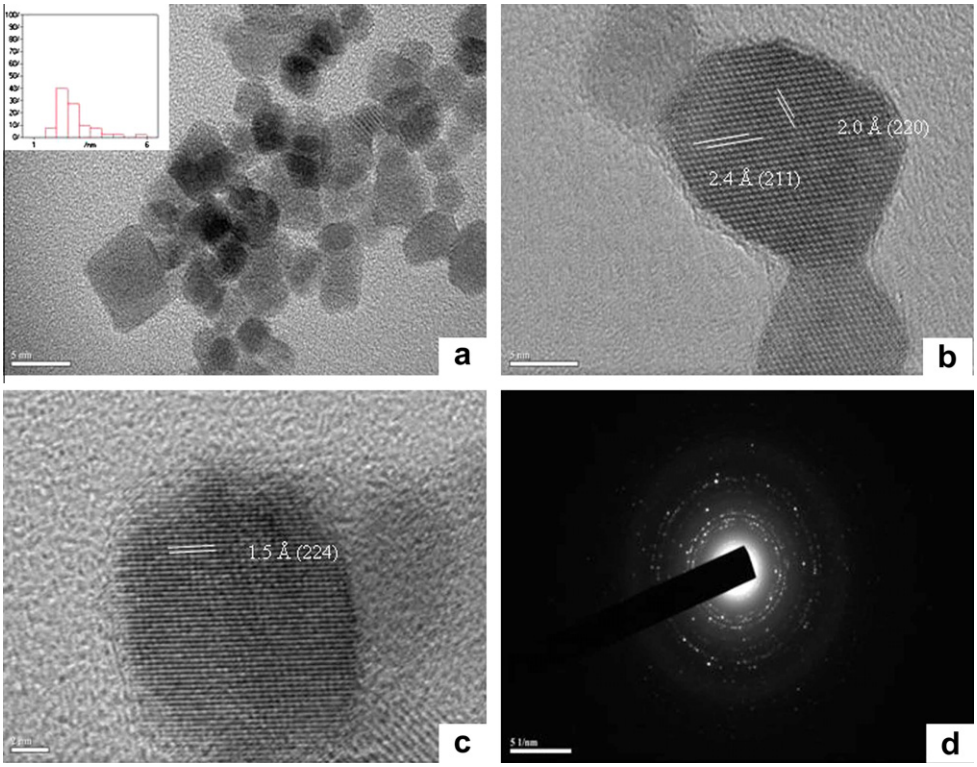

Fig. 5. (a) HRTEM, (b, c) lattice image, and (d) SAED pattern of Mn_3O_4 nanocrystal using conventional method (NaOH).

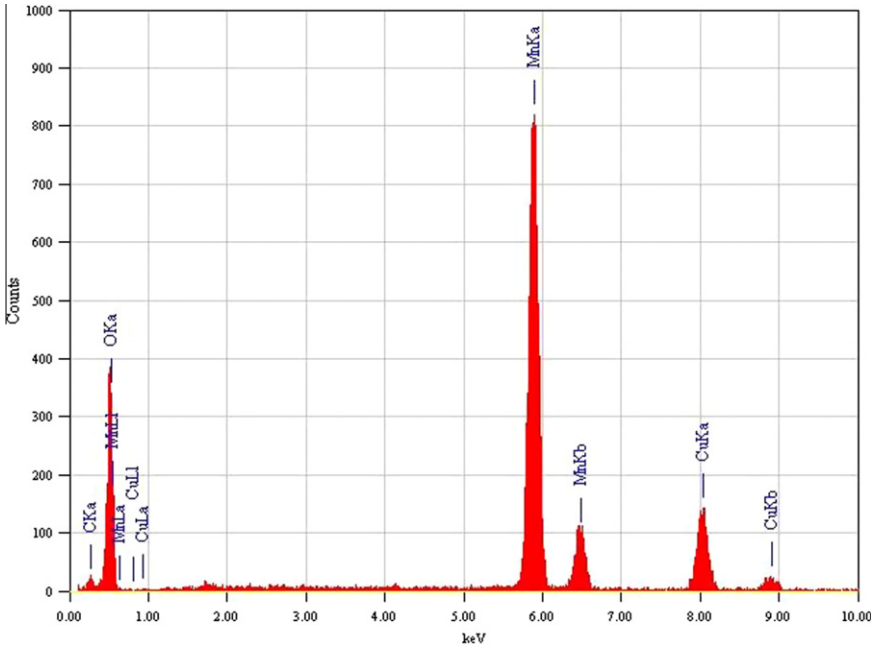

Fig. 6. EDS pattern of Mn_3O_4 nanocrystal using conventional method (NaOH).

According to the TEM images for the samples prepared with HMT in the presence of ultrasonic irradiation (Fig. 7), the amount of nanorods was less than with NaOH. The average size of nanoparticles was about 15 nm and the shape was nearly cubic. The diameter for nanorods was 50 nm and the length was about a few micrometers. The size of nanoparticles and nanorods were larger than the samples obtained by NaOH. This behavior could be explained based on the chemical decomposition of HMT to ammonium and hydroxide ions in water. The chemical decomposition of HMT in the presence of ultrasonic irradiation was measured (Supplementary Fig. S5). Based on this Figure, the decomposition was gradually increased with time up to 40 min and then it was reached to an approximate constant amount. It is proposed that the gradual release of ammonium and subsequent OH^{-1} ions in

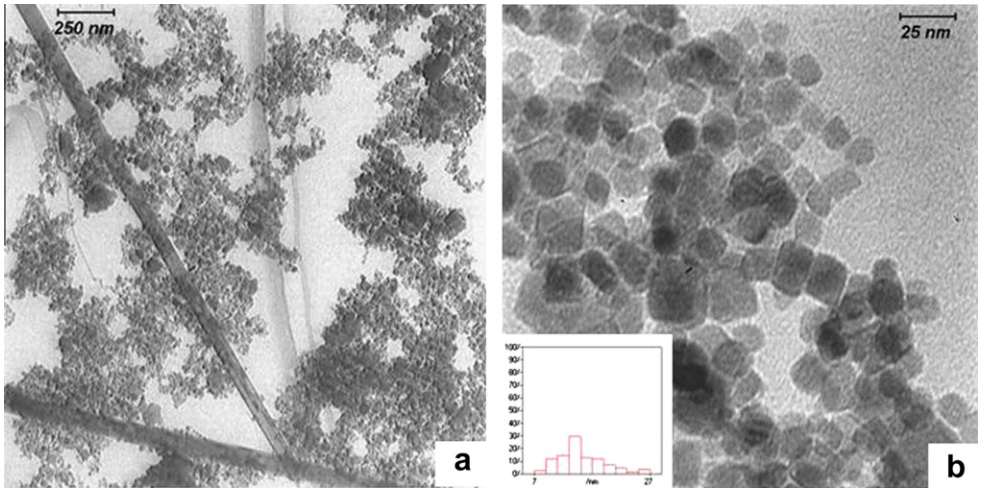

Fig. 7. TEM image and size distribution of Mn_3O_4 nanocrystal using ultrasonic irradiation (HMT).

the solution led to slower nucleation and growth process and this causes an increase on the size of nanoparticles and nanorods.

3.4. Magnetic measurements

It is known that the physical properties of materials are related to their morphologies and sizes. The magnetic properties of Mn_3O_4 nanocrystals (mixture of nanorod and nanoparticles) prepared in the presence of ultrasonic irradiation with NaOH have been studied by measuring the magnetization as a function of temperature; field-cooled (FC) with field of 1000 Oe and zero-field-cooled (ZFC). The magnetization-temperature curves are shown in Fig. 8a. It is revealed that the magnetization decreases by increasing the temperature up to 39 K and then sharply decreases around 44 K. The magnetization almost disappeared in the range of 44–295 K. It is suggested that the increasing of thermal energy especially above the T_c led to fluctuation of magnetic moment of nanoparticles and decrease of magnetization. The transition temperature, T_c, can be determined through the derivative of magnetizations with respect to the temperature which is given in Fig. 8b. The T_c was found at 40 K which is lower than the observed temperature for the bulk of Mn_3O_4 (43 K) [77,78]. The lower value of the ferrimagnetic onset temperature (T_c) as compared to the reported value for the bulk indicates the particles are single domain in nature. This result is consistent with the linear relationship between crystal volume V and blocking temperature T_B as predicted from the equation:

$$kV = 25k_BT_B \quad (5)$$

K is the anisotropy constant and k_B is Boltzmann's constant [79]. Therefore, the T_c or T_B reduces with decrease of size and similar trend was also observed in the literature [58].

Gopalakrishnan et al. [63] reported the synthesis of nanocrystalline Mn_3O_4 by high intensity ultrasonic irradiation and showed that the T_c for nanoparticles with sizes of 15 nm was 39 K. Qian and co-workers [80] synthesized nanorod Mn_3O_4 using PEG-20000 with diameter of about 100 nm and lengths up to 15–20 μm and showed that the T_c for nanorod was 41 K. They suggested that the shape anisotropy of products have a little influence on T_c value [80]. In our case, it is proposed that the mixture of nanoparticles and nanorods led to a lower value of T_c than the results obtained by Qian and co-workers. Also, the smaller size of nanorods in our case may affect on the lower value of T_c.

Generally, a bulk ferrimagnetic compound is multidomain in nature below its ferrimagnetic transition temperatures. The multidomain character of a ferrimagnetic system can be lost if the particle size decreases to below a critical size. The same as bulk ferrimagnetic systems, the single domain ferrimagnetic systems

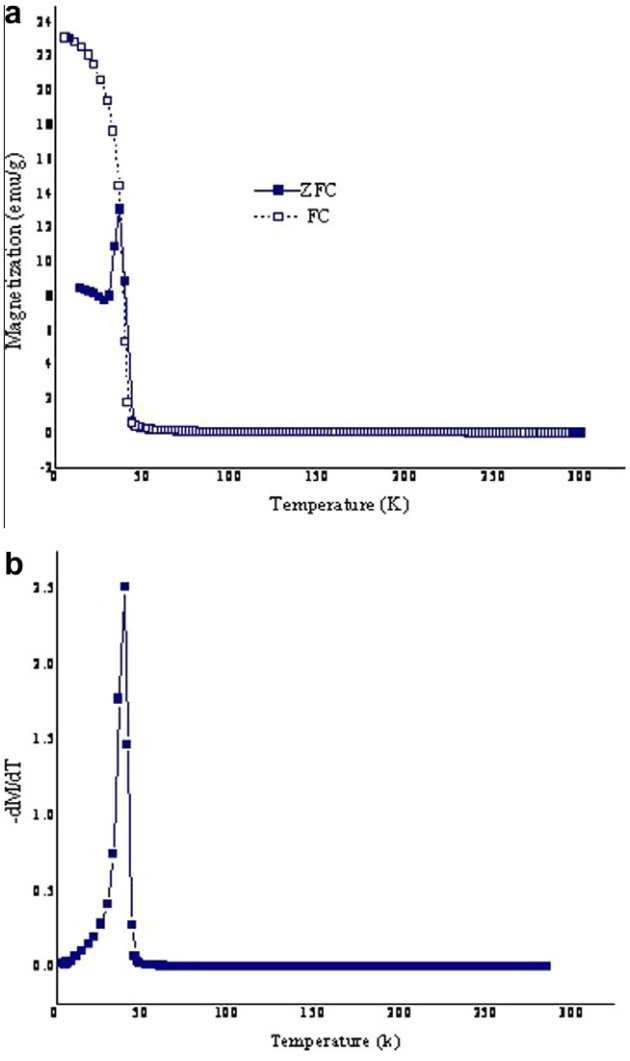

Fig. 8. (a) M-T curve of Mn_3O_4 nanocrystal using ultrasonic irradiation and (b) temperature derivative of magnetization vs. temperature.

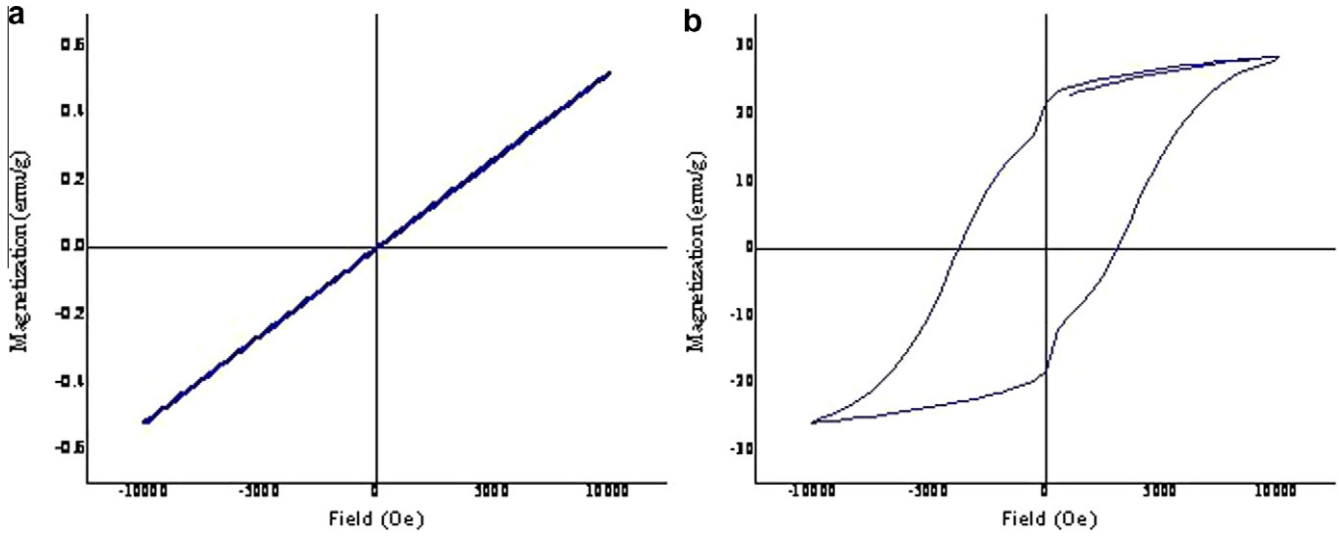

Fig. 9. Hysteresis loop of Mn_3O_4 nanocrystal using ultrasonic irradiation (NaOH): (a) room temperature and (b) 10 K.

also show a hysteresis in their *M–H* (magnetization vs. field measurement) behavior. The sample shows an obvious ferrimagnetic behavior at low temperature.

The magnetization curve of sample at room temperature is shown in Fig. 9a. The *M–H* curve is linear with the field and has no coercivity at room temperature. The hysteresis in the single-domain ferrimagnetic particles vanishes when the particle size becomes so small that the maximum anisotropy energy becomes close to the thermal energy. In this case, the process of flipping of the single-domain spin becomes uninhibited [53]. This state of ferrimagnetism called "superparamagnetism" as it does not show any hysteresis in its *M–H* behavior and the magnetization never get saturated even at very high applied field. In the present case, the room temperature magnetization curve shows no hysteresis which indicates the superparamagnetic character of the sample. It has also claimed that the nanorods can exhibit a superparamagnetic behavior [80,81]. The saturated magnetization (M_s) was not reached even at 10 kOe applied magnetic field and the maximum value of magnetization was 0.5 emu/g in the field of 10 kOe. A large coercivity and hysteresis loop were observed at temperature below T_c (10 K) (Fig. 9b). The maximum value for magnetization in 10 K was about 28.4 emu/g at 10 kOe. The coeresivity and remnant were 3514 Oe and 22 emu/g, respectively. The obtained data exhibit smaller coercivity in comparison with the value reported by Qian and co-workers (6177 Oe) [80] and a similar coercivity for the Mn_3O_4 as a film (3500 Oe) [82]. The smaller coercivity may be related to the mixture of nanorods and nanoparticles in the products.

3.5. Proposed mechanism

Aqueous solutions of manganese(II) salts in the presence of strong bases form the pink-colored, insoluble manganese(II) hydroxide, $Mn(OH)_2$. In the presence of air and oxygen, $Mn(OH)_2$ is gradually oxidized to form dark-brown products which contains $Mn(OH)_3$ or possibly MnO, and MnO_2 nH_2O. Manganese(II) hydroxide is a fairly weak base and when heated in the presence of air, it forms Mn_3O_4 [34].

The chemical reactions driven by ultrasonic waves can occur in three different regions [83,84]: (a) the inner environment of the collapsing bubble (gas phase), where high temperatures and pressures are produced and causing the pyrolysis of water into H and OH radicals, (b) the interfacial region between the cavitation bubbles and bulk solution, and (c) the bulk of the solution. The temperature in case (b) is lower than the case (a) but, the temperature is still high enough to rupture chemical bonds. In the bulk solution, the reaction between reactant molecules and OH or H radicals produced by the cavitation can take place at the medium temperatures.

In this case, it is known that the sonochemical reaction does not occur inside the cavity which is due to the ionic structure of initial reactants (manganese acetate). Therefore the reaction can facilitate in interface of the bubble or in the bulk of the solution. A suggested mechanism for the formation of Mn_3O_4 from aqueous manganese acetate in the presence of O_2 molecules are as following:

$$Mn(CH_3COO)_2 \overset{H_2O}{\rightarrow} Mn^{2+} + 2CH_3COO^- \quad (6)$$

$$H_2O \overset{)))))}{\rightarrow} H^{\cdot} + OH^{\cdot} \quad (7)$$

According to Okitsu et al. [85], OOH radicals are formed by the reaction of H radicals with O_2 molecules under the air atmosphere and then the recombination of OOH radicals proceed to form H_2O_2:

$$H^{\cdot} + O_2 \rightarrow {}^{\cdot}OOH \quad (8)$$

$$2{}^{\cdot}OOH \rightarrow H_2O_2 + O_2 \quad (9)$$

The oxidant generated by ultrasound can be used in reaction (10):

$$3Mn^{+2} + 6CH_3COO^- + H_2O_2 + 2H_2O \rightarrow Mn_3O_4 + 6CH_3COOH \quad (10)$$

In the basic solution, the following reactions can also be occurred:

$$3Mn^{2+} + 6OH^- + \frac{1}{2}O_2 \rightarrow Mn(OH)_2 + 2MnOOH + H_2O \quad (11)$$

$$Mn(OH)_2 + 2MnOOH \rightarrow Mn_3O_4 + 2H_2O \quad (12)$$

4. Conclusion

In summary, this work was focused on the synthesis of Mn_3O_4 nanocrystal under mild conditions. The pure phase of Mn_3O_4 was synthesized by ultrasonic bath with low intensity of irradiation and conventional method by using manganese acetate as a precursor in the presence of NaOH and HMT at pH 8.0. The results in the presence and absence of ultrasound were compared. Under ultrasound a mixture of nanorods and nanoparticle with nearly cubic

in shape were observed. But, in the conventional method, there was not observed any nanorods. The absence of the rod-like structure in the conventional method might be attributed to the capping agent like NaOH on the interface of nanoparticles. However, the desorption of capping agent from the surface of nanoparticles under ultrasonic irradiation and effective collision of nanoparticles could be led to production of 1-D structure. The magnetization measurements showed that the nanopowders were single domain in nature with the observation of superparamagnetic behavior at room temperature.

Acknowledgments

We would like to thank Dr. Shizhang Qiao and Dr. Muxina Konarova (ARC Centre of Excellence for Functional Nanomaterials, Australian Institute for Bioengineering and Nanotechnology, The University of Queensland) for helpful assistance in the evaluation of magnetic properties, HRTEM analysis and Mrs. R. Pesyan from Central Research Laboratory of Ferdowsi University of Mashhad for TEM analysis.

Appendix A. Supplementary data

Supplementary data associated with this article can be found, in the online version, at doi:10.1016/j.ultsonch.2011.10.012.

References

[1] E. Grootendorst, Y. Verbeek, V. Ponce, The role of the mars and van krevelen mechanism in the selective oxidation of nitrosobenzene and the deoxygenation of nitrobenzene on oxidic catalysts, J. Catal. 157 (1995) 706–712.
[2] H. Gleiter, Nanostructured materials: basic concepts and microstructure, Acta Mater. 48 (2000) 1–29.
[3] D.G. Mitchell, MR imaging contrast agents — what's in a name?, J Magn. Reson. Imaging 7 (1997) 1–4.
[4] A. Jordan, R. Scholz, K. Maier-Hauff, M. Johannsen, P. Wust, J. Nadobny, H. Schirra, H. Schmidt, S. Deger, S. Loening, W. Lanksch, R. Felix, Presentation of a new magnetic field therapy system for the treatment of human solid tumors with magnetic fluid hyperthermia, J. Magn. Magn. Mater. 225 (2001) 118–126.
[5] M.E. McHenry, D.E. Laughlin, Nano-scale materials development for future magnetic applications, Acta Mater. 48 (2000) 223–238.
[6] B.D. Cullity, Introduction to Magnetic Materials, Addison, Wesley, Reading,, MA, USA, 1972.
[7] L. Chen, T. Horiuchi, T. Mori, Catalytic reduction of NO over a mechanical mixture of $NiGa_2O_4$ spinel with manganese oxide: influence of catalyst preparation method, Appl. Catal. A 209 (2001) 97–105.
[8] J.H. Wu, S.P. Ko, H.L. Liu, S.S. Kim, J.S. Ju, K.K. Young, Sub 5 nm Fe_3O_4 nanocrystals via coprecipitation method, Colloids Surf. A 313–314 (2008) 268–272.
[9] D.C. Niu, Y.S. Li, Z. Ma, H. Diao, J.L. Gu, H.R. Chen, W.R. Zhao, M.L. Ruan, Y.L. Zhang, J.L. Shi, Preparation of uniform, water-soluble, and multifunctional nanocomposites with tunable sizes, Adv. Funct. Mater. 20 (2010) 773–780.
[10] W.D. Zhang, H.M. Xiao, L.P. Zhu, S.Y. Fu, Template-free solvothermal synthesis and magnetic properties of novel single-crystalline magnetite nanoplates, J. Alloys Compd. 477 (2009) 736–738.
[11] D. Amara, I. Felner, I. Nowik, S. Margel, Synthesis and characterization of Fe and Fe_3O_4 nanoparticles by thermal decomposition of tri iron dodecacarbonyl, Colloids Surf. A 339 (2009) 106–110.
[12] J. Lu, X.L. Jiao, D.R. Chen, W. Li, Solvothermal synthesis and characterization of Fe_3O_4 and γ-Fe_2O_3 nanoplates, J. Phys. Chem. C 113 (2009) 4012–4017.
[13] H.F. Zhou, R. Yi, J.H. Li, Y. Su, X.H. Liu, Microwave-assisted synthesis and characterization of hexagonal Fe_3O_4 nanoplates, Solid State Sci. 12 (2010) 99–104.
[14] M. Sivakumar, A. Towata, K. Yasui, T. Tuziuti, Y. Iida, A new ultrasonic cavitation approach for the synthesis of zinc ferrite nanocrystals, Curr. Appl. Phys. 6 (2006) 591–593.
[15] W.H. Suh, K.S. Suslick, Magnetic and porous nanospheres from ultrasonic spray Pyrolysis, J. Am. Chem. Soc. 127 (2005) 12007–12010.
[16] R.A. Caruso, M. Ashokkumar, F. Grieser, Sonochemical formation of colloidal platinum, Colloids Surf. A 169 (2000) 219–225.
[17] A. Pradhan, R.C. Jones, D. Caruntu, C.J. O'Connor, M.A. Tarr, Gold–magnetite nanocomposite materials formed via sonochemical methods, Ultrason. Sonochem. 15 (2008) 891–897.
[18] V. Kesavan, P.S. Sivanand, S. Chandrasekaran, Y. Koltypin, A. Gedanken, Catalytic aerobic oxidation of cycloalkanes with nanostructured amorphous metals and alloys, Angew. Chem., Int. Ed. 38 (1999) 3521–3523.
[19] J.H. Bang, K.S. Suslick, Applications of ultrasound to the synthesis of nanostructured materials, Adv. Mater. 22 (2010) 1–21.
[20] M. Sivakumar, A. Gedanken, D. Bhattacharya, I. Brukental, Y. Yeshurun, W. Zhong, Y.W. Du, I. Felner, I. Nowik, Sonochemical synthesis of nanocrystalline rare earth orthoferrites using $Fe(CO)_5$ precursor, Chem. Mater. 16 (2004) 3623–3632.
[21] J.H. Bang, K.S. Suslick, Sonochemical synthesis of nanosized hollow hematite, J. Am. Chem. Soc. 129 (2007) 2242–2243.
[22] Y. Jin, P. Wang, D. Yin, J. Liu, L. Qin, N. Yu, G. Xie, B. Li, Gold nanoparticles prepared by sonochemical method in thiol-functionalized ionic liquid, Colloids Surf. A 302 (2007) 366–370.
[23] D. Zhang, X. Zhang, X. Ni, J. Song, H. Zheng, Low-temperature fabrication of $MnFe_2O_4$ octahedrons: magnetic and electrochemical properties, Chem. Phys. Lett. 426 (2006) 120–123.
[24] J. Lao, J. Huang, D. Wang, Z. Ren, Self-assembled In_2O_3 nanocrystal chains and nanowire networks, Adv. Mater. 16 (2004) 65–69.
[25] Y. Li, M. Sui, Y. Ding, G. Zhang, J. Zhuang, C. Wang, Preparation of $Mg(OH)_2$ nanorods, Adv. Mater. 12 (2000) 818–821.
[26] Y-W. Jun, M.F. Casula, J-H. Sim, S.Y. Kim, J. Cheon, A.P. Aliyisatos, Surfactant-assisted elimination of a high energy facet as a means of controlling the shapes of TiO_2 nanocrystals, J. Am. Chem. Soc. 125 (2003) 15981–15985.
[27] B. Li, Y. Zhao, X. Xu, H. Zhou, B. He, Z. Wu, Z. Zhang, A simple method for the preparation of containing Sb nano- and microcrystallines via an ultrasound agitation, Ultrason. Sonochem. 14 (2007) 557–562.
[28] H. Liu, H. Cui, F. Han, X. Li, J. Wang, R.I. Boughton, Growth of Bi_2Se_3 nanobelts synthesized through a co-reduction method under ultrasonic irradiation at room temperature, Cryst. Growth Des. 5 (2005) 1711–1714.
[29] S-M. Zhou, X-H. Zhang, X-M. Meng, X. Fan, S-T. Lee, S-K. Wu, Sonochemical synthesis of mass single-crystal PbS nanobelts, J. Solid State Chem. 178 (2005) 399–403.
[30] H. Li, H. Li, Z. Guo, Y. Liu, The application of power ultrasound to reaction crystallization, Ultrason. Sonochem. 13 (2006) 359–363.
[31] N. Amara, B. Ratsimba, A. Wilhelm, H. Delmas, Growth rate of potash alum crystals comparison of silent and ultrasonic conditions, Ultrason. Sonochem. 11 (2004) 17–21.
[32] E.J.W. Verwey, E.L. Helimann, Physical properties and cation arrangement of oxides with spinel structures I. cation arrangement in spinels, J. Chem. Phys. 15 (1947) 174–180.
[33] A.P. Ramirez, Strongly geometrically frustrated magnets, Annu. Rev. Mater. Sci. 24 (1994) 453–480.
[34] S.B. Parker, McGraw-Hill Encyclopedia of Chemistry, McGraw Hill, New York, 1983.
[35] R. Regmi, R. Tackett, G. Lawes, Suppression of low-temperature magnetic state in Mn_3O_4 nanoparticles, J. Magn. Magn. Mater. 321 (2009) 2296–2299.
[36] A.R. Armstrong, P.G. Bruce, Synthesis of layered $LiMnO_2$ as an electrode for rechargeable lithium batteries, Nature 381 (1996) 499–500.
[37] Y.F. Shen, R.P. Zerger, R.N. Deguzman, S.I. Suib, L. Mccurdy, D.I. Potter, C.I. Oyoung, Manganese oxide octahedral molecular sieves: preparation, Characterization, and applications, Science 260 (1993) 511–515.
[38] M.C. Bernrad, H.L. Goff, B.B. Thi, Electrochromic reactions in manganese oxides, J. Electrochem. Soc. 140 (1993) 3065–3070.
[39] A.H. De Vries, L. Hozoi, R. Broer, Importance of interatomic hole screening in core-level spectroscopy of transition metal oxides: 3*s* hole states in MnO, Phys. Rev. B 66 (2002) 035108–035118.
[40] Y. Yamashita, K. Mukai, J. Yoshinobu, M. Lippmaa, T. Kinoshita, M. Kawasaki, Chemical nature of nanostructures of $La_{0.6}Sr_{0.4}MnO_3$ on $SrTiO_3$ (100), Surf. Sci. 514 (2002) 54–59.
[41] Y.C. Zhang, T. Qiao, X.Y. Hu, Preparation of Mn_3O_4 nanocrystallites by low-temperature solvothermal treatment of γ-MnOOH nanowires, J. Solid State Chem. 177 (2004) 4093–4097.
[42] E.R. Stobble, B.A. Boer, J.W. Geus, The reduction and oxidation behavior of manganese oxides, Catal. Today 47 (1999) 161–167.
[43] W. Weimin, Y. Yongnian, Z. Jiayu, Selective reduction of nitrobenzene to nitrosobenzene over different kinds of trimanganese tetroxide catalysts, Appl. Catal. A 133 (1995) 81–93.
[44] E.J. Grootendorst, Y. Verbeek, V. Ponec, The role of the Mars and Van Krevelen mechanism in the selective oxidation of nitrosobenzene and the deoxygenation of nitrobenzene on oxidic catalysts, J. Catal. 157 (1995) 706–712.
[45] T. Yamashita, A. Vannice, NO decomposition over Mn_2O_3 and Mn_3O_4, J. Catal. 163 (1996) 158–168.
[46] G. Marbán, T. Valdés-Solís, A.B. Fuertes, Mechanism of low-temperature selective catalytic reduction of NO with NH_3 over carbon-supported Mn_3O_4 role of surface NH_3 species: SCR mechanism, J. Catal. 226 (2004) 138–155.
[47] M. Baldia, F. Milellab, G. Ramisb, V.S. Escribano, G. Bu, An FT-IR and flow reactor study of the selective catalytic oxy-dehydrogenation of C3 alcohols on Mn_3O_4, Appl. Catal., A 166 (1998) 75–88.
[48] C.H. Hare, M.G. Fernald, Effect of prime pigment on metal primer performance, Mod. Paint Coat. 74 (1984) 40–46.
[49] L. Sánchez, J. Farcy, J-P. Pereira-Ramos, L. Hernán, J. Morales, J.L. Tirado, Low-temperature mixed spinel oxides as lithium insertion compounds, J. Mater. Chem. 6 (1996) 37–39.
[50] K.A.M. Ahmed, Q. Zeng, K. Wu, K. Huang, Mn_3O_4 nanoplates and nanoparticles: Synthesis, characterization, electrochemical and catalytic properties, J. Solid State Chem. 183 (2010) 744–751.

[51] J. Pike, J. Hanson, L. Zhang, S.-W. Chan, Synthesis and redox behavior of nanocrystalline Hausmannite (Mn_3O_4), Chem. Mater 19 (2007) 5609–5619.
[52] S. Ching, J.L. Roark, N. Duan, S.L. Suib, Sol–Gel route to the tunneled manganese oxide cryptomelane, Chem. Mater. 9 (1997) 750–754.
[53] T. Ozkaya, A. Baykal, H. Kavas, Y. Koseoglu, M.S. Toprak, A novel synthetic route to Mn_3O_4 nanoparticles and their magnetic evaluation, Physics B 403 (2008) 3760–3764.
[54] X. Li, L. Zhou, J. Gao, H. Miao, H. Zhang, J. Xu, Synthesis of Mn_3O_4 nanoparticles and their catalytic applications in hydrocarbon oxidation, Powder Technol. 190 (2009) 324–326.
[55] Z.W. Chen, J.K.L. Lai, C.H. Shek, Shape-controlled synthesis and nanostructure evolution of single-crystal Mn_3O_4 nanocrystals, Scr. Mater. 55 (2006) 735–738.
[56] Z. Yang, Y. Zhang, W. Zhang, X. Wang, Y. Qian, X. Wen, S. Yang, Nanorods of manganese oxides: synthesis, characterization and catalytic application, J. Solid State Chem. 179 (2006) 679–684.
[57] F. Li, J. Wu, Q. Qin, Z. Li, X. Huang, Facile synthesis of γ-MnOOH micro/nanorods and their conversion to β-MnO_2, Mn_3O_4, J. Alloys compd. 492 (2010) 339–346.
[58] W.S. Seo, H.H. Jo, K. Lee, B. Kim, S.J. Oh, J.T. Park, Size-dependent magnetic properties of colloidal Mn_3O_4 and MnO nanoparticles, Angew. Chem. 116 (2004) 1135–1137.
[59] B. Yang, H. Hu, C. Li, X. Yang, Q. Li, Y. Qian, One-step route to single-crystal γ-Mn_3O_4 nanorods in alcohol–water system, Chem. Lett. 33 (2004) 804.
[60] A. Vázquez-Olmos, R. Redón, G. Rodríguez-Gattorno, M.E. Mata-Zamora, F. Morales-Leal, A.L. Fernández-Osorio, J.M. Saniger, One-step synthesis of Mn_3O_4 nanoparticles: structural and magnetic study, J. Colloid Interf. Sci. 291 (2005) 175–180.
[61] L-X. Yang, Y. Liang, H. Chen, Y-F. Meng, W. Jiang, Controlled synthesis of Mn_3O_4 and $MnCO_3$ in a solvothermal system, Mater. Res. Bull. 44 (2009) 1753–1759.
[62] L. Sicard, J-M. LeMeins, C. Methivier, F. Herbst, S. Ammar, Polyol synthesis and magnetic study of Mn_3O_4 nanocrystals of tunable size, J. Magn. Magn. Mater. 322 (2010) 2634–2640.
[63] I.K. Gopalakrishnan, N. Bagkar, R. Ganguly, S.K. Kulshreshtha, Synthesis of superparamagnatic Mn_3O_4 nanocrustallites by ultrasonic irradiation, J. Cryst. Growth 280 (2005) 436–441.
[64] T. Rohani Bastami, M.H. Entezari, Sono-synthesis of Mn_3O_4 nanoparticles in different media without additives, Chem. Eng. J. 164 (2010) 261–266.
[65] V. Ganesh Kumar, D. Aurbuch, A. Gedanken, A comparison between hot-hydrolysis and sonolysis of various Mn(II) salts, Ultrason. Sonochem. 10 (2003) 17–23.
[66] L. A. Crum, T. J. Mason, J. L. Reisse, K. S. Suslick, Sonochemistry and sonoluminesence, Kluwer Academic Publishers, Washington, USA, 1999,p. 248.
[67] T.J. Mason, Sonochemistry, Oxford University Press, New York, 1999.
[68] S. Vajnhandi, A.M. Le Marechal, Case study of the sonochemical discoloration of textile azo dye reactive blue 5, J. Hazard. Mater. 141 (2007) 329–335.
[69] R.H. Leonard, Quantitative range of nessler's reaction with ammonia, Clin. Chem. 9 (1963) 417–422.
[70] P. Niedzielski, I. Kurzyca, J. Siepak, A new tool for inorganic nitrogen speciation study: simultaneous determination of ammonium ion, Nitrite and nitrate by ion chromatography with post-column ammonium derivatization by Nessler reagent and diode-array detection in rain water samples, Anal. Chim. Acta 577 (2006) 220–224.
[71] M. Ishii, M. Nakahira, Infrared absorption spectra and cation distributions in $(Mn, Fe)_3O_4$, Solid State Commun. 11 (1972) 209–212.
[72] Y. Wang, J. Zhang, Y. Yang, F. Huang, J. Zheng, D. Chen, F. Yan, Z. Lin, C. Wang, NaOH concentration effect on the oriented attachment growth kinetics of ZnS, J. Phys. Chem. B 111 (2007) 5290–5294.
[73] J. Zhang, Z. Lin, Y. Lan, G. Ren, D. Chen, F. Huang, M. Hong, A multistep oriented attachment kinetics: coarsening of ZnS nanoparticle in concentrated NaOH, J. Am. Chem. Soc. 128 (2006) 12981–12987.
[74] Z.A. Peng, X. Peng, Mechanisms of the shape evolution of CdSe nanocrystals, J. Am. Chem. Soc. 123 (2001) 1389–1395.
[75] E.J.H. Lee, C. Ribeiro, E. Longo, E.R. Leite, Oriented attachment: an effective mechanism in the formation of anisotropic nanocrystals, J. Phys. Chem. B 109 (2005) 20842–20846.
[76] C. Ribeiro, E.J.H. Lee, E. Longo, E.R. Leite, A kinetic model to describe nanocrystal growth by the oriented attachment mechanism, Chem. Phys. Chem. 6 (2005) 690–696.
[77] G. Srinivasan, M.S. Seehra, Magnetic properties of Mn_3O_4 and a solution of the canted-spin, Phys. Rev. B 28 (1983) 1–7.
[78] Y.Q. Chang, X.Y. Xu, X.H. Luo, C.P. Chen, D.P. Yu, Synthesis and characterization of Mn_3O_4 nanoparticles, J. Cryst. Growth 264 (2004) 232–236.
[79] C.P. Bean, J.D. Livingston, Superparamagnetism, J. Appl. Phys. 30 (1959) 120S–129S.
[80] J. Du, Y. Gao, L. Chai, G. Zou, Y. Li, Y. Qian, Hausmannite Mn_3O_4 nanorods: synthesis, characterization and magnetic properties, Nanotechnology 17 (2006) 4923–4928.
[81] L. Sicard, J-M. Le Meins, C. Methivier, F. Herbst, S. Ammar, Polyol synthesis and magnetic study of Mn_3O_4 nanocrystals of tunable size, J. Magn. Magn. Mater. 322 (2010) 2634–2640.
[82] L.W. Guo, D.L. Peng, H. Makino, K. Inaba, H.J. Ko, K. Sumiyama, T. Yao, Structural and magnetic properties of Mn_3O_4 films grown on MgO(0 0 1) substrates by plasma-assisted MBE, J. Magn. Magn. Mater. 213 (2000) 321–325.
[83] R.V. Kumar, Y. Diamant, A. Gedanken, Sonochemical synthesis and characterization of nanometer-size transition metal oxides from metal acetates, Chem. Mater. 12 (2000) 2301–2305.
[84] T.J. Mason, Advances in Sonochemistry, JAI Press, London, 1993.
[85] K. Okitsu, K. Iwasaki, Y. Yobiko, H. Bandow, R. Nishimura, Y. Maeda, Sonochemical degradation of azo dyes in aqueous solution: a new heterogeneous kinetics model taking into account the local concentration of OH radicals and azo dyes, Ultrason. Sonochem. 12 (2005) 255–262.